J. Fluid Mech. (1969), *vol.* 39, *part* 1, *pp.* 25–48
Printed in Great Britain

Experiments on the instability of stratified shear flows: immiscible fluids

By S. A. THORPE
National Institute of Oceanography, Wormley, Godalming, Surrey

(Received 8 November 1968 and in revised form 4 June 1969)

When a long rectangular tube containing two immiscible fluids is slightly tilted away from the horizontal, a uniformly accelerating flow is produced with shear at the interface. The presence of shear leads to instability, which is characterized by the spontaneous and rapid growth of almost stationary waves if the fluid depths are equal and the density difference small. The conditions for the onset of Kelvin–Helmholtz instability, taking account of the accelerating flow and the presence of a velocity transition region at the interface, are investigated theoretically and comparison made with observations. The time at which instability occurs is quite well predicted by this theory, but the wavelength of the unstable waves is rather greater than predicted in the accelerating flow. The difference between the predictions and observations may be the result of finite amplitude effects or of the development of Tollmien–Schlichting instability before Kelvin–Helmholtz.

1. Introduction

In a paper published in 1968, which is hereafter referred to as I, we described a technique, first used by Osborne Reynolds, to produce a stratified shear flow under fully controlled conditions. The flow is produced by tilting a long horizontal tube, of rectangular section and completely filled with the stratified fluid, through a small angle. In the uniformly accelerating flow which follows, the velocity of the fluid near the centre of the tube is parallel to the tube walls and depends on the initial density distribution. This flow is eventually disrupted either by the spontaneous growth of waves and a transition to turbulence, or by the arrival of surges which develop and propagate from the ends of the tube. In the experiments and theory described in this paper the tank is filled with two immiscible fluids, and the density distribution when the tube is first tilted is

$$\rho(z) = \begin{cases} \rho_1 & (0 < z < h_1), \\ \rho_2 & (-h_2 < z < 0), \end{cases} \tag{1.1}$$

where z is measured normal to the initially horizontal walls of the tube located at $z = -h_2, h_1$ (figure 1). At the interface ($z = 0$) there is surface tension, γ. A theory is developed to predict the onset of instability of the uniformly accelerating flow in the tube and the wavelength of the instability. The experiments allow some comparison between prediction and observation, and show how the

instability develops at large amplitude well beyond the region of validity of the theory.

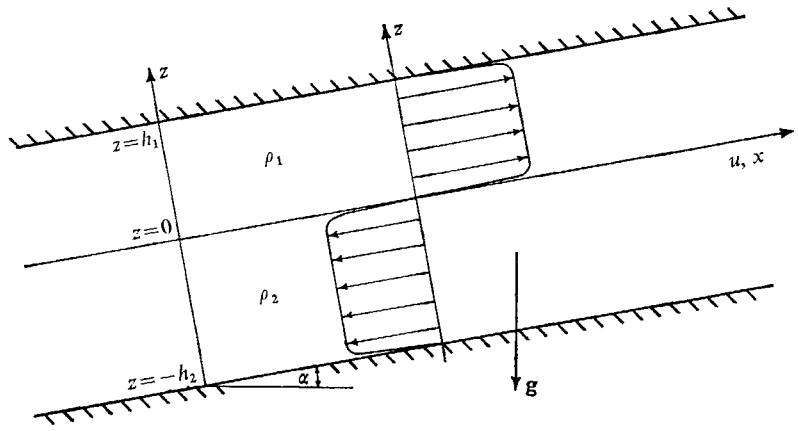

FIGURE 1. Notation in the tilted tube.

The velocity distribution which arises when the tube is tilted is characterized by a sharp shear layer at the interface. In the absence of viscosity it may easily be shown that the velocity, u, parallel to the tube walls up the line of greatest slope (the x direction) is

$$u = \begin{cases} U_1 = \dfrac{(\rho_2-\rho_1)\,h_2 tg \sin\alpha}{\rho_1 h_2+\rho_2 h_1} & (0 < z < h_1), \\ U_2 = \dfrac{(\rho_2-\rho_1)\,h_1 tg \sin\alpha}{\rho_1 h_2+\rho_2 h_1} & (-h_2 < z < 0) \end{cases} \tag{1.2}$$

(I, equation (7)), where α is the angle of inclination of the tube to the horizontal and g is the acceleration due to gravity. The presence of viscosity affects the flow near the walls and the interface, but, if instability occurs soon after the tube has been tilted (and typically in the experiments it occurs within the first 3 sec) the influence of viscosity on most of the velocity profile in the parallel accelerating flow is slight. A typical velocity profile is shown in figure 1.

The spontaneous growth of waves at a short time after the tube was tilted is shown in figure 8 (plate 1) and is described in § 3. The theoretical results derived in § 2 are compared with observations in § 3.

There appear to be two possible instabilities, the Kelvin–Helmholtz and the Tollmien–Schlichting, which might account for the first development of waves, but we shall discuss here only the former instability. (The various types of instability have been discussed and classified by Benjamin (1960, 1963) and Landahl (1962).) It is quite possible that a Tollmien–Schlichting instability develops at an earlier stage than the Kelvin–Helmholtz,† and the results therefore place

† Benjamin (1963) has shown that a Tollmien–Schlichting (class A) instability will occur when the velocity difference across the interface is only $1/\sqrt{2}$ times that necessary for the development of Kelvin–Helmholtz (class C) instability, provided that the density difference at the interface is small. The growth rate of the Tollmien–Schlichting instability is, however, much less than that of the Kelvin–Helmholtz, and it is probable that the observed instability belongs to the latter category.

only an *upper bound* on the times at which instability occurs. The maximum Reynolds number, based on the displacement thickness of a boundary layer, which occurs in the experiments before the onset of instability, is 183, which is somewhat below the critical value 575, estimated by Schlichting (see Schlichting 1955) for the onset of instability on a rigid wall. It would therefore seem that the development of Tollmien–Schlichting instability on the walls of the tube is unlikely. No similar conclusion can be reached about instability at the interface, which may be characterized by a smaller critical Reynolds number.

2. Theory

2.1. *Discussion*

The stability of the steady flow of two deep immiscible fluids, each moving in the same direction parallel to the interface and each having constant velocity and density, the lighter fluid above, was examined theoretically by Kelvin (1871). For sufficiently small differences in the velocities above and below the interface, there are no growing wave-like disturbances of any wave-number. As the velocity difference, ΔU, is increased, at first one wave-number, k_c, and then a range of wave-numbers containing k_c become unstable. It was found that the critical wave-number

$$k_c = \sqrt{[g(\rho_2 - \rho_1)/\gamma]} \tag{2.1}$$

and the steady velocity difference, ΔU_c, at which instability first occurs is

$$\Delta U_c = \left\{2\frac{\rho_1+\rho_2}{\rho_1\rho_2}\sqrt{[g(\rho_2-\rho_1)\gamma]}\right\}^{\frac{1}{2}}, \tag{2.2}$$

where ρ_1 is the density of the upper fluid, ρ_2 that of the lower, and γ is the interfacial surface tension.

Holmboe (1962) examined the stability of an infinite fluid of density

$$\rho = \begin{cases} \rho_1 & (0 < z), \\ \rho_2 & (0 > z), \end{cases} \tag{2.3a}$$

with the continuous velocity distribution

$$u = \begin{cases} U & (d < z), \\ Uz/d & (-d < z < d), \\ -U & (-d > z), \end{cases} \tag{2.3b}$$

but with no surface tension at the interface, and found that there was instability over a range of wave-numbers at each value of the velocity difference, $2U$.

An extension of Holmboe's work to include the effects of interfacial tension yields a critical wave-number but one which is modified by the value of the non-dimensional parameter $\gamma/[gd^2(\rho_2-\rho_1)]$, and this is discussed in detail in § 2.5. Because of the effects of viscosity the flow in the experiments has not the discontinuous profile of (1.2), but changes continuously at the interface (§ 2.4).

Although (2.3) does not represent the actual velocity distribution in the experiments, the results described in § 2.5 are helpful in assessing the effect of a gradual transition in velocity at the interface on the conditions at the onset of instability and will be used in § 3. (A far more sophisticated theory is that developed by Lock (1954) specifically to examine the generation of water waves at an air/water interface by the flow of air over water, but it does not appear profitable to modify his theory for the present range of quite small density differences, as this would involve considerable labour and it is doubtful whether it would substantially improve the theoretical estimates of the conditions at the onset of instability.)

The development of a stability theory for a viscous accelerating fluid, such as we have in the experiments, has not proved possible by analytical methods. However, the stability of small disturbances to the flow defined by (1.1) and (1.2) have been considered (§ 2.3); this is equivalent to an examination of the effect of acceleration on the flow studied by Kelvin. When this effect has been examined (and the presence of boundaries at finite distances) and the effect of a gradual transition in the (quasi-steady) velocity at the interface assessed, corrections may be made to the values of k_c and ΔU_c of (2.1) and (2.2) respectively and these corrected values compared with the observations.

2.2. *Steady flow*

Consider a fluid of density given by (1.1) with $h_1 = h_2 = h$, and with the steady velocity distribution

$$u = \begin{cases} \Delta U/2, & 0 < z < h, \\ -\Delta U/2, & -h < z < 0, \end{cases} \tag{2.4}$$

and surface tension γ at the interface, $z = 0$. When small disturbances to the interface proportional to $\exp(ikx+pt)$ are examined, it is found that the dispersion relation is

$$p = \frac{ik\Delta U(\rho_2-\rho_1)}{2(\rho_1+\rho_2)} \pm \left\{\frac{k^2(\Delta U)^2\rho_1\rho_2}{(\rho_1+\rho_2)^2} - \frac{[\gamma k^3 + gk(\rho_2-\rho_1)]\tanh kh}{\rho_1+\rho_2}\right\}^{\frac{1}{2}}. \tag{2.5}$$

For a growing disturbance p must contain a real positive part; that is,

$$(\Delta U)^2 > \frac{\rho_1+\rho_2}{\rho_1\rho_2}\left[\gamma k + \frac{g}{k}(\rho_2-\rho_1)\right]\tanh kh. \tag{2.6}$$

For deep fluids the right-hand side of this expression has a minimum at a wave-number $k = k_c$, the critical wave-number, when

$$k_c = \sqrt{[g(\rho_2-\rho_1)/\gamma]}$$

and thus the minimum value of the velocity difference for a growing disturbance is

$$\Delta U_c = \left\{2\frac{\rho_1+\rho_2}{\rho_1\rho_2}\sqrt{[g(\rho_2-\rho_1)\gamma]}\right\}^{\frac{1}{2}}$$

as found by Kelvin, see (2.1), (2.2).

If now

$$l = k[\gamma/g(\rho_2-\rho_1)]^{\frac{1}{2}}, \quad r = h[g(\rho_2-\rho_1)/\gamma]^{\frac{1}{2}}$$

and $$J = \frac{2}{(\Delta U)^2}\frac{\rho_1+\rho_2}{\rho_1\rho_2}[g\gamma(\rho_2-\rho_1)]^{\frac{1}{2}},$$

the condition (2.6) becomes

$$1 > \frac{J}{2l}(1+l^2)\tanh rl, \tag{2.7}$$

and figure 2 shows the curves of l against J for $1 = (J/2l)(1+l^2)\tanh rl$ and for various r.

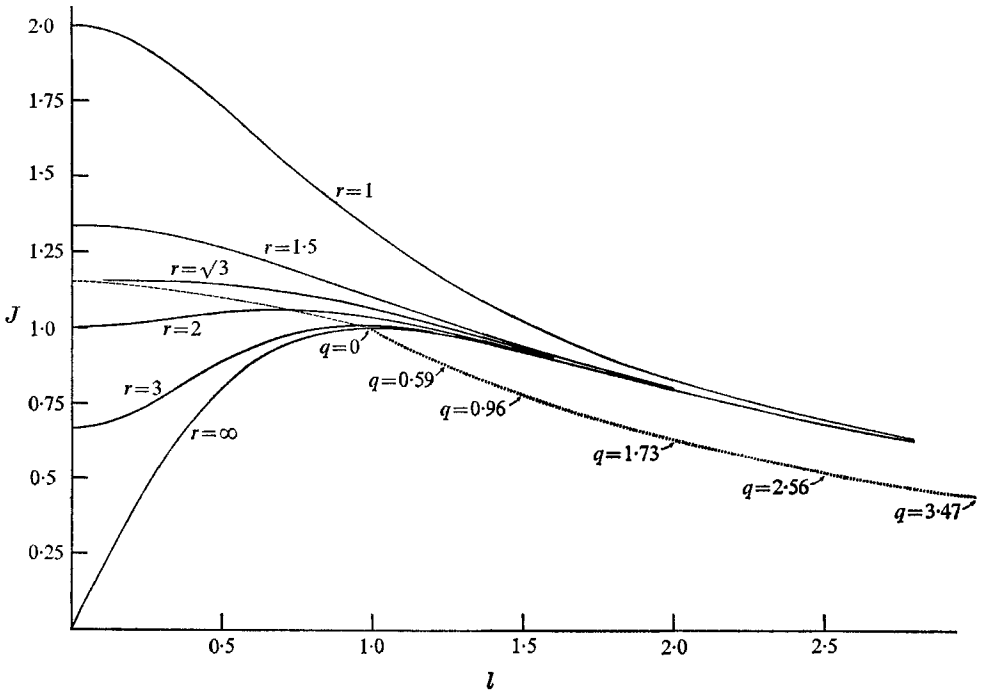

FIGURE 2. The variations of J with l at various r (full curves); the variation of the maximum J for each r with l (dashed curve); and the variation of maximum J for each q with l (dotted curve).

It will be seen that the non-dimensionalized wave-number, l, for which J is largest (and therefore ΔU is least) decreases as r (and therefore h) decreases, but that the largest value of J does not vary very much from its value for very large r until $r < \sqrt{3}$. Hence the effect of the boundaries is to increase the critical wave-number to a value above that for infinite depth, but not to change the critical velocity difference substantially, unless

$$h < \sqrt{3}\{\gamma/[g(\rho_2-\rho_1)]\}^{\frac{1}{2}}.$$

(The analysis when h takes such small values is inappropriate and a long-wave approximation is more suitable.) The dashed curve in figure 2 shows the locus of largest J for various r. If r is known (and it will be imposed by the conditions

of the experiments), the corresponding largest J, and therefore ΔU_c, is found, and also the corresponding l, and therefore k_c, is known.

For deep fluids ($r \to \infty$) the real part of p may be written

$$\mathscr{R}(p) = q\left\{\frac{g^3(\rho_2-\rho_1)^3}{(\rho_1+\rho_2)^2\gamma}\right\}^{\frac{1}{4}},$$

where

$$q^2 = l^2[2/J - (l + 1/l)].$$

The curve $q = 0$ is the continuous curve marked $r = \infty$ in figure 2. The curves for $q \neq 0$ lie below this. The dotted line lying below the curve $r = \infty$ in figure 2 is the locus of points of the maximum J on the set of curves q = constant. Some values of q are marked. This dotted curve indicates the wave-numbers of the disturbances which have the largest growth rates for any given value of the stability parameter J. The trend towards higher wave-numbers as J decreases shows that unstable flows (for which ΔU exceeds ΔU_c) have a fastest growing wave-number which exceeds k_c. This result anticipates a similar result which will be found for uniformly accelerating flows.

2.3. *The effect of acceleration*

We wish to consider small disturbances to the basic state given by (1.1) and (1.2). The motions in both the upper and lower fluids are started from rest† and are therefore irrotational. We can therefore define velocity potentials $\phi_1(x, z, t)$, $\phi_2(x, z, t)$ so that

$$\nabla^2\phi_i = 0 \quad (i = 1, 2) \tag{2.8}$$

and the fluid velocity is

$$\mathbf{u} = \begin{cases} U_1\mathbf{i} + \nabla\phi_1, & \xi(x,t) < z < h_1, \\ U_2\mathbf{i} + \nabla\phi_2, & -h_2 < z < \xi(x,t), \end{cases} \tag{2.9}$$

where $\xi(x, t)$ is the position of the interface at position x measured along the tank and at time t and $\mathbf{i} = (1, 0, 0)$. The observed instability is found to be approximately two-dimensional (at least when the disturbance is small) and we therefore consider only disturbances which are functions independent of y. This assumption is justified in appendix B, where it is shown that the most rapidly growing disturbance is two-dimensional. The width of the tank is supposed to be large and in the experiments is over six times the fluid depths.

The boundary conditions are that the velocity normal to the tube boundaries vanishes

$$\frac{\partial\phi_1}{\partial z} = 0 \quad \text{at} \quad z = h_1, \quad \frac{\partial\phi_2}{\partial z} = 0 \quad \text{at} \quad z = -h_2; \tag{2.10}$$

the kinematic condition at the interface

$$\left(\frac{D}{Dt}\right)_1 \xi = \frac{\partial\phi_1}{\partial z}, \quad \left(\frac{D}{Dt}\right)_2 \xi = \frac{\partial\phi_2}{\partial z} \quad \text{at} \quad z = \xi, \tag{2.11}$$

where

$$\left(\frac{D}{Dt}\right)_j \equiv \frac{\partial}{\partial t} + (U_j\mathbf{i} + \nabla\phi_j)\nabla \quad (j = 1, 2); \tag{2.12}$$

† When the tube is suddenly tilted to inclination α no Rayleigh–Taylor instability is observed.

and the condition on the pressures at the interface

$$p_1 - p_2 = \gamma/R \quad \text{at} \quad z = \xi, \tag{2.13}$$

where p_1 is the pressure in the upper fluid and p_2 that in the lower, and R is the radius of curvature of the interface. The pressure is given by the linearized Bernoulli equation

$$\frac{p_i}{\rho_i} + \frac{\partial}{\partial t}(U_i x) + \frac{\partial}{\partial t}\phi_i + U_i \frac{\partial \phi_i}{\partial x} + gx \sin\alpha + gz\cos\alpha = A_i(t) \quad (i = 1, 2) \tag{2.14}$$

(where there is no summation over a repeated suffix).

The method of solving the linearized form of the equations (2.8)–(2.14) is described in detail in appendix A. A solution is found which is periodic in the x direction with wave-number k. (A general solution may be found by superposition in the usual way.) The solution for the disturbance to the interface $\xi(x, t)$ is best expressed in the form

$$\xi(x, t) = \mathscr{R}\{N(\tau) \exp[i(kx + \beta t^2)]\}, \tag{2.15}$$

where

$$\tau = \left\{\frac{2kg \sin\alpha(\rho_2 - \rho_1)(h_1 + h_2)\sqrt{(T_1 T_2 \rho_1 \rho_2)}}{(\rho_1 h_2 + \rho_2 h_1)(\rho_1 T_2 + \rho_2 T_1)}\right\}^{\frac{1}{2}} t, \tag{2.16}$$

$$\beta = -\frac{k(\rho_2 - \rho_1) g \sin\alpha(\rho_1 h_2 T_2 - \rho_2 h_1 T_1)}{2(\rho_1 T_2 + \rho_2 T_1)(\rho_1 h_2 + \rho_2 h_1)} \tag{2.17}$$

and $T_i = \tanh kh_i$, $i = 1, 2$, and $\mathscr{R}$ indicates that the real part is to be taken. $N(\tau)$ satisfies the equation

$$\frac{d^2 N}{d\tau^2} - (a + \tfrac{1}{4}\tau^2) N = 0, \tag{2.18}$$

where

$$a = -\frac{[\gamma k^2 + (\rho_2 - \rho_1) g \cos\alpha](\rho_1 h_2 + \rho_2 h_1)\sqrt{(T_1 T_2)}}{2g \sin\alpha(\rho_2 - \rho_1)(h_1 + h_2)\sqrt{(\rho_1 \rho_2)}}. \tag{2.19}$$

Equation (2.18) is a standard form of the equation for the parabolic cylinder function. Two linearly independent solutions, $U(a, \tau)$, $V(a, \tau)$, are known. For $a < 0$, as it is here, U is bounded and oscillatory for all $\tau > 0$ and tends to zero as τ tends to infinity, whilst V is oscillatory and bounded for $\tau < 2\sqrt{(-a)}$ and increases monotonically for $\tau > 2\sqrt{(-a)}$;

$$V(a, \tau) \sim \sqrt{\left(\frac{2}{\pi}\right)} \frac{\exp(\frac{1}{4}\tau^2)}{\tau^{(\frac{1}{2}-a)}} \tag{2.20}$$

as $\tau \to \infty, \tau \gg |a|$. The condition $\tau = 2\sqrt{(-a)}$ is in fact equivalent to the condition in steady flow for the onset of instability. The wave-number k_c for the smallest $\tau\,(=\tau_c)$ for which $\tau = 2\sqrt{(-a)}$ is satisfied (and therefore the earliest time $t = t_c$ at which $\tau = 2\sqrt{(-a)}$), is given by (2.1) if the fluid depths are very large, and the corresponding velocity difference is given by (2.2). Hence the conditions for the onset of instability in a steady flow (that is for the growth of a disturbance of some wave-number) also serve as the condition for the first growth of a wave in the accelerating flow.

However, it is not clear that the wave which will be first *observed* in the experiments will have the critical wave-number predicted in § 2.2. Even ignoring the changes in wave-number which may result at finite amplitude, the observed wave will depend upon the spectrum of the background 'noise' and upon which wave-numbers grow most rapidly. There is no information available at present about the background noise spectrum in the experiments. Before an experiment is made, the tube is left in a horizontal position for at least five minutes until no motion can be observed. At the start of an experiment one end of the tube is raised sharply until it comes into contact with a buffer. The impulse from this contact produces some small capillary ripples at the interface which originate at the side walls and which disappear rapidly and well before the onset of the

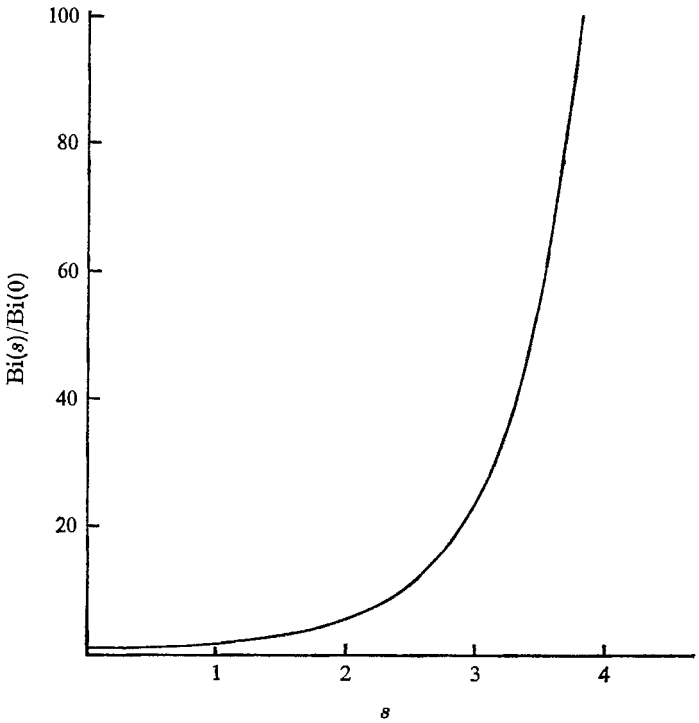

FIGURE 3. The growth of a disturbance; the variation of Bi(s)/Bi(0) with s.

shear instability. Further experiments are planned to study the growth of a known initial disturbance made by producing standing or progressive waves in the tube, but we shall suppose here that the noise level is fairly uniform in the neighbourhood of the most rapidly growing waves. Even with this rather sweeping assumption we are left in a quandary. It is now possible to estimate the wave-number of the wave which first increases its amplitude by, say, 10 times, but without knowledge of the amplitude of the initial disturbance we cannot tell what growth is necessary before the wave becomes visible (or measurable), and the first wave to increase its amplitude by 10 times may not be that to increase

first by, say, 100 times. We can, however, examine the solution for ξ near $\tau = 2\sqrt{(-a)}$ to see how rapidly wave growth will occur, and to compare the solution for the accelerating fluid with that made on a quasi-static approximation, and to see whether the observed wave-number should be greater or less than k_c predicted in § 2.2.

In (2.18) write

$$\tau = 2\sqrt{(-a)} + \tau_1. \tag{2.21}$$

Then

$$\frac{d^2N}{d\tau_1^2} = (\tau_1\sqrt{(-a)} + \tfrac{1}{4}\tau_1^2)\,N, \tag{2.22}$$

or approximately, if $\tau_1 \ll 4\sqrt{(-a)}$,

$$\frac{d^2N}{d\tau_1^2} = \tau_1\sqrt{(-a_1)}\,N, \tag{2.23}$$

which transforms into

$$\frac{d^2N}{ds^2} = sN, \tag{2.24}$$

when

$$s = (-a)^{\frac{1}{6}}\tau_1. \tag{2.25}$$

This is the equation for the linearly independent Airy functions Ai (s), Bi (s). Ai (s) is a monotonic function decreasing to zero as $s \to \infty$ whilst Bi (s) is monotonic increasing to infinity. We are here looking for a growing disturbance and, having no knowledge of conditions at $s = 0$, will suppose that $N(s) = \mathrm{Bi}\,(s)/\mathrm{Bi}\,(0)$. The curve $N(s)$ is shown in figure 3. Tenfold growth will have occurred when s is approximately 2·46 and 100-fold growth at s equals 3·83, provided that

$$|3{\cdot}83(-a)^{-\frac{1}{6}}| \ll |4(-a)^{\frac{1}{2}}|$$

so that the conditions for the validity of the approximation are satisfied. The approximation made here is satisfied for large values of a, typically when $|(-a)^{\frac{3}{2}}| \gg 1$. This condition will be satisfied when $\sin\alpha$ is small, since a contains $\sin\alpha$ in its denominator. Numerical comparison of the approximate solution (the solution of (2.23)) with the exact solution to (2.18) (based on the tables for the parabolic cylinder function given by Abramowitz & Stegun 1965) shows that even when $\sqrt{(-a)}$ is as small as $\frac{1}{2}$, the time of 100-fold growth is predicted to within 3·5 %. We shall therefore use the approximate solution for comparison with observations.

A comparison of the predicted growth of the disturbance at the interface when the fluid is accelerating and that predicted on the assumption that the growth rate is at each instant given by (2.5), a quasi-static approximation, is made in appendix C. The time at which a disturbance will grow to 100 times its initial amplitude is underestimated by less than 10 % by the quasi-static approximation.

Growth of disturbances is very rapid once 100-fold growth has been achieved (500-fold growth occurs when $s = 4{\cdot}64$) and it seems likely that a good estimate of the observed wavelength may be given if we use for comparison the wave which will first grow to 100 times its initial amplitude.

Now at 100-fold growth, from (2.21) and (2.25),

$$\tau = 2(-a)^{\frac{1}{2}} + 3{\cdot}83(-a)^{\frac{1}{3}}, \tag{2.26}$$

and with substitution from (2.16) and (2.19) the time at 100-fold growth is

$$t_{100} = A\left\{\left[\frac{(1+l^2)\tanh lr}{l}\right]^{\frac{1}{2}} + \frac{B}{[l^3(1+l^2)\tanh lr]^{\frac{1}{3}}}\right\}, \tag{2.27}$$

where $$A = \left[\frac{(\rho_1+\rho_2)^3 h\cos\alpha}{4gr\sin^2\alpha(\rho_2-\rho_1)\rho_1\rho_2}\right]^{\frac{1}{2}}, \quad B = 1{\cdot}91\left[\frac{4(\rho_1\rho_2)^{\frac{1}{2}}\tan\alpha}{\rho_1+\rho_2}\right]^{\frac{2}{3}},$$

$$l = k\left[\frac{\gamma}{g\cos\alpha(\rho_2-\rho_1)}\right]^{\frac{1}{2}} \quad \left(=\frac{k}{k_c}\right)$$

and $$r = \left[\frac{g\cos\alpha(\rho_2-\rho_1)}{\gamma}\right]^{\frac{1}{2}} h.$$

(These variables are the same as those defined in § 2.2 but now with reduced gravity, $g\cos\alpha$.)

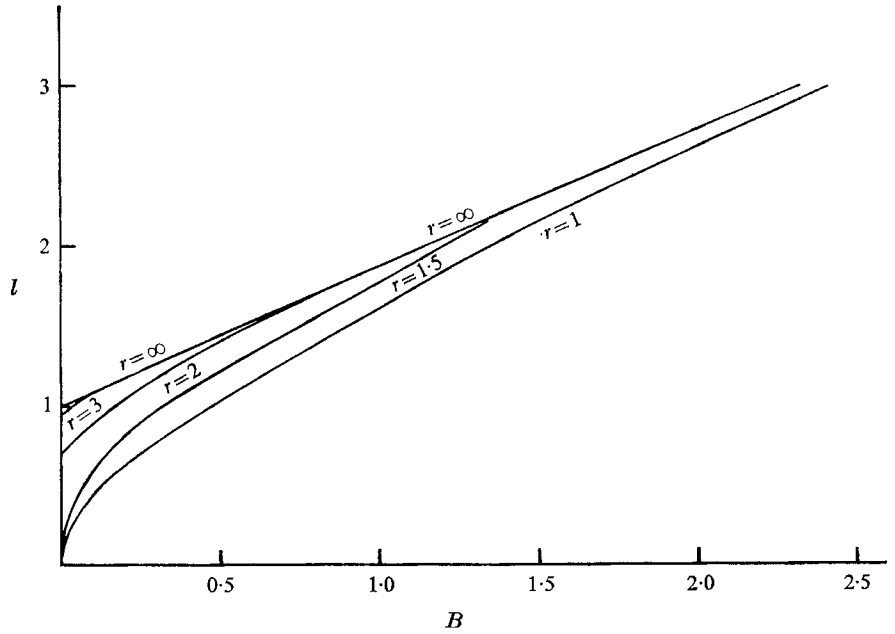

FIGURE 4. The variation of l with B for various r at the time at which 100-fold growth occurs.

When B is very small the minimum value of t_{100} is given by finding the minimum of the first term in the curly brackets in (2.27), and this is exactly the same as the problem of finding the maximum J considered in § 2.2. The non-dimensional wave-numbers l for various τ are given by the points on the dotted curve in figure 2.

The minimum value of t_{100}, found by differentiating (2.27), occurs when

$$B = \frac{3(l^2-1)(1+l^2)^{\frac{2}{3}}\tanh^{\frac{1}{3}} rl + 3rl(1+l^2)^{\frac{1}{3}}\tanh^{\frac{2}{3}} rl\,\mathrm{sech}^2 rl}{(3+5l^2)\tanh rl + rl(1+l^2)\,\mathrm{sech}^2 rl} \tag{2.28}$$

and the corresponding values of l and B for various r are shown in figure 4. The effect of acceleration is to *increase* the wave-number of the most rapidly growing wave to a value above that predicted by steady flow. For fixed values of r and h, the wave-number which first increases its amplitude by one hundred times, k_{100}, increases as B increases and therefore as α increases. For $2{\cdot}3 > B > 0{\cdot}1$, to a good approximation the curves $r = 3$, $r = \infty$ are given by

$$l = 1 + 0{\cdot}86B. \tag{2.29}$$

Typical values of r and B in the experiments are 3 and 0·5 respectively, and the wave-number k_{100} may be significantly increased by the effect of acceleration. The first wave to increase its amplitude by 100 times for these values of r and B corresponds to $l = 1{\cdot}43$ (compared with $l = 0{\cdot}95$ in the non-accelerating flow) and the time of 100-fold growth, t_{100}, for this wave is $1{\cdot}807A$. For $l = 1{\cdot}20$, $t_{100} = 1{\cdot}821A$ and for $l = 1{\cdot}70$, $t_{100} = 1{\cdot}818A$. Since these values do not differ greatly from that corresponding to $l = 1{\cdot}43$, a range of wave-numbers are all subject to rapid growth at about the same time. In such conditions it is to be expected that there will be considerable scatter in the wavelengths observed in the experiments, but that the time of the onset of instability may be well predicted. The spectrum of the background noise in the neighbourhood of the fastest growing wave may have a profound influence on the observed wavelengths. What actually happens will be described later.

2.4. *Diffusion of vorticity in the accelerating flow*

Due to the presence of viscosity, the flow in the neighbourhood of the interface is not given by the discontinuous profile (1.2) but there exists a boundary-layer flow, the thickness of which grows with time. (There are similar boundary layers at the walls of the tube but these are not considered here.) If ν_1, ν_2 are the values of the coefficient of kinematic viscosity in the upper and lower fluids respectively and u_1, u_2, the corresponding fluid speeds in the fluids, then it may be shown that, well away from the walls of the tube,

$$u_i = (-1)^{1+i} g \sin\alpha \frac{\rho_2-\rho_1}{\rho_1+\rho_2}\left\{t\,\mathrm{erf}\left[\frac{z}{2\sqrt{(\nu_i t)}}\right] - \frac{z^2}{2\nu_i}\mathrm{erfc}\left[\frac{z}{2\sqrt{(\nu_i t)}}\right] + z\left(\frac{t}{\pi\nu_i}\right)^{\frac{1}{2}}\exp\left[-\frac{z^2}{4\nu_i t}\right]\right\} \quad (i = 1, 2), \tag{2.30}$$

where

$$\mathrm{erfc}\,x = 1 - \mathrm{erf}\,x = \frac{2}{\sqrt{\pi}}\int_x^\infty e^{-t^2}\,dt,$$

provided that the fluid depths are equal and large in comparison with $\max_{i=1,2}(\pi\nu_i t)^{\frac{1}{2}}$ and that

$$\left(\frac{\nu_1}{\nu_2}\right)^{\frac{1}{2}}\frac{\rho_1}{\rho_2} = 1.\dagger$$

† In the experiments with a density difference of 0·22 g cc^{-1} described in § 3, the ratio $(\nu_1/\nu_2)^{\frac{1}{2}}(\rho_1/\rho_2)$ was estimated and found to be 1·07.

If $\nu = \frac{1}{2}(\nu_1+\nu_2)$, an approximation to the profile at time t is

$$u = \begin{cases} g\sin\alpha\left(\frac{\rho_2-\rho_1}{\rho_1+\rho_2}\right)t; & z > \frac{1}{2}(\pi\nu t)^{\frac{1}{2}}, \\ 2g\sin\alpha\left(\frac{\rho_2-\rho_1}{\rho_1+\rho_2}\right)\left(\frac{t}{\pi\nu}\right)^{\frac{1}{2}}z; & -\frac{1}{2}(\pi\nu t)^{\frac{1}{2}} < z < \frac{1}{2}(\pi\nu t)^{\frac{1}{2}}, \\ -g\sin\alpha\left(\frac{\rho_2-\rho_1}{\rho_1+\rho_2}\right)t; & -\frac{1}{2}(\pi\nu t)^{\frac{1}{2}} > z. \end{cases} \tag{2.31}$$

(This has approximately the same gradient at $z = 0$ and the same speed for large $|z|$.) The stability of a steady profile of this type is considered in § 2.5 to assess the effect of the viscous modification of the flow profile.

2.5. *The effect of a gradual velocity transition*

We now examine the stability of the steady flow of an infinite fluid with velocity distribution given by (2.3*b*) and density by (2.3*a*) with surface tension γ at the density discontinuity, in order to assess the effect of the gradual transition in velocity near the interface resulting from the viscous diffusion of vorticity across the interface in the experiments. The analysis is similar to that carried out by Holmboe (1962) in the solution of the problem without surface tension, the only difference being that there is now a discontinuity in the pressure of the fluids across the interface and a boundary condition (2.13) is applied. An interfacial disturbance is found having the form

$$\zeta(x,t) = \mathscr{R}\{a_1\exp[ik(x-ct)]\},$$

where c is a root of a quartic equation which may be written in the form

$$\chi(v) \equiv v^4-(\mu^2+P)v^2+\mu^2Q+\delta v(Rv^2+S) = 0, \tag{2.32}$$

where

$$v = c/U, \quad \mu^2 = \frac{g\delta}{U^2k}\left[1+\frac{k^2\gamma}{g(\rho_2-\rho_1)}\right],$$

$$P = 1-\frac{1}{kd}+\frac{\tanh kd}{(kd)^2(1+\tanh kd)}, \quad Q = \left[1-\frac{\tanh kd}{kd(1+\tanh kd)}\right]^2,$$

$$R = \frac{2\tanh kd}{kd(1+\tanh kd)}, \quad S = -\frac{Q}{kd} \quad \text{and} \quad \delta = \frac{\rho_1-\rho_2}{\rho_1+\rho_2}.$$

The disturbance will grow if c contains a positive imaginary part and the onset of instability is characterized by this condition on c.

Suppose first that δ is very small and may be neglected in (2.32) whilst μ^2 remains of order unity. Then (2.32) reduces to the form

$$\chi_1(v) \equiv v^4-(\mu^2+\rho)v^2+\mu^2Q = 0, \tag{2.33}$$

which has a double root v_1 if $\chi_1(v_1) = 0$ and $d\chi_1/dv = 0$ at $v = v_1$. The condition for these equations to be satisfied simultaneously is

$$(\mu^2+P)^2 = 4\mu^2Q \tag{2.34}$$

and $v_1^2 = 2\mu^2 Q/(\mu^2+P)$, if $\mu^2 Q \neq 0$. (Both μ^2 and Q are positive and non-zero here.) Since $\chi_1(v) = \chi_1(-v)$ and $d\chi_1/dv = 0$ at $v = 0$, a small disturbance of the parameters P and Q will produce four real roots for c or two pairs of complex conjugate roots. Hence (2.34) is the condition for marginal stability. The solution of (2.34) is $\mu = \mu_0$ say, where

$$\mu_0^2 = 2Q - P \pm 2\sqrt{(Q^2 - QP)}. \tag{2.35}$$

$Q^2 - QP$ is always positive, as may be shown by substituting values in terms of kd. It was shown by Holmboe (1962) (for $\gamma = 0$) that instability is for values of μ^2 in the region between the two roots of (2.35). P and Q are specified by kd, and the two critical roots of μ^2 can be found from (2.35). If we write

$$\mu^2 = \frac{J_1}{kd}(1+\sigma kd), \tag{2.36}$$

where $$J_1 = \frac{g\delta d}{U^2} \quad \text{and} \quad \sigma = \frac{\gamma}{d^2 g(\rho_2 - \rho_1)},$$

the variation of the critical values of J_1 (when $\mu^2 = \mu_0^2$) with kd for various σ may be found. Since instability occurs in that region between the two roots of μ_0^2 and the minimum velocity difference across the layer ($2U$) to give instability is given by the largest value of J_1 (and hence the largest value of μ^2), the onset of instability as $2U$ increases is characterized by μ_0^2 taking the value of the higher root when the positive sign is taken in (2.35). The corresponding variation of J_1 with kd for various σ is shown by the curves labelled $\delta = 0$ in figure 5. The parameter σ is equal to $1/(dk_c)^2$, where k_c, given by (2.1), is the critical wave-number in the problem when $d = 0$, and the values of dk_c for each σ are indicated by the vertical arrows on the kd axis in figure 5. They lie very close to but slightly above the values of kd for which J_1 has a maximum value and the critical wave-number is therefore slightly overestimated by (2.1) when δ is very small. The values of the J_1 based on the assumption that the velocity difference across the interface is given by ΔU_c in (2.2) (the critical difference as d tends to zero) are

$$J_1 (= J_{1c}) = (1-\delta^2)/(2\sigma^{\frac{1}{2}})$$

and this tends to $1/(2\sigma^{\frac{1}{2}})$ as δ tends to zero. These values of J_1 for various σ are marked on the J_1 axis in figure 5 by horizontal arrows and are seen to lie above the maximum values given by the curves. Hence the velocity differences required for marginal stability are increased by the presence of a gradual transition in velocity at the interface.

When δ is small compared with unity, but not negligible, we must reconsider the solution by (2.32). Suppose $\chi = 0$ has a double root v_2. Then $d\chi/dv = 0$ at $v = v_2$ and

$$\chi(v) - \frac{v}{4}\frac{d\chi}{dv} = -\tfrac{1}{2}(\mu^2+P)v_2^2 + \mu^2 Q + \tfrac{1}{4}\delta v_2 (Rv_2^2 + 3S)$$

$$= 0 \quad \text{at} \quad v = v_2.$$

Hence $$v_2^2 = \frac{2\mu^2 Q}{\mu^2+P}(1+\epsilon) \quad (= v_1^2(1+\epsilon)), \tag{2.37}$$

where $$\mu^2 Q\epsilon = \frac{\delta}{4}\left(\frac{2\mu^2 Q}{\mu^2+P}\right)^{\frac{1}{2}}\left[\frac{2R\mu^2 Q}{\mu^2+P}+3S\right] \tag{2.38}$$

neglecting higher-order terms in δ.

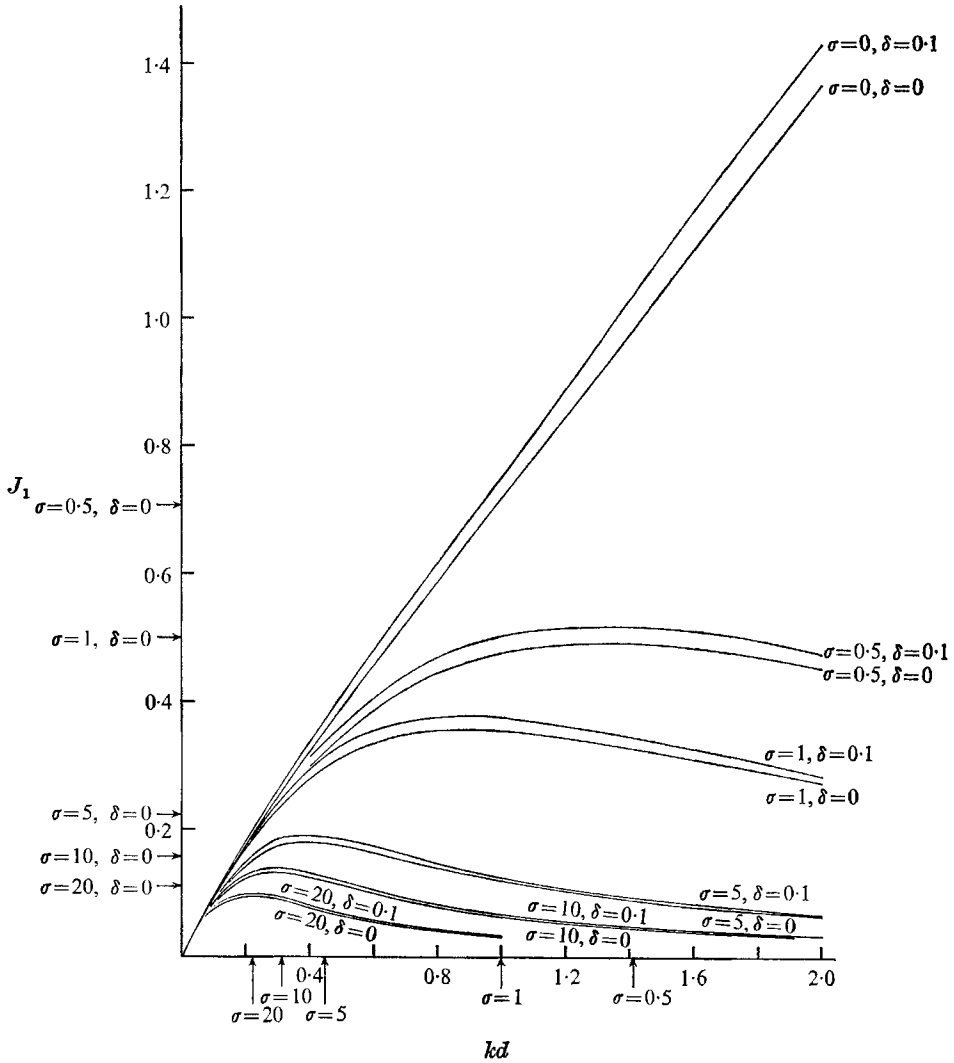

FIGURE 5. The variation of J_1 with kd for various r and for $\delta = 0$, $\delta = 0{\cdot}1$. The arrows marked on the axes are explained in the text.

Substituting now for v_2 from (2.37) into (2.32) and again neglecting second-order terms in δ we find $$\mu^2 = \mu_0^2(1+\epsilon_1),$$

where $$\epsilon_1 = \frac{\delta}{(\mu_0^2-Q)^{\frac{1}{2}}Q^{\frac{1}{2}}\mu_0^{\frac{3}{2}}}(\mu_0 Q^{\frac{1}{2}}R+S)$$

and μ_0 is a root of (2.34). As before the largest root of (2.34) is that which characterizes the conditions of critical velocity difference. The stability curves for $\delta = 0{\cdot}1$ are also shown in figure 5. The critical wave-numbers are still well predicted by (2.1) but the velocity difference for marginal stability is underestimated by (2.2); the smaller is σ, the greater is the underestimate.

In the experiments the values of δ lie between 0 and 0·125 and σ based on a value of $d = \frac{1}{2}(\pi\nu t)^{\frac{1}{2}}$ (see (2.31)), has a value of about $25/t$ (where t is in seconds). At the onset of instability, t varies between 0·5 and 3·0 sec and so the critical velocity difference, and therefore the time of onset of instability, may be underestimated by as much as 10 % by the theory which supposes that an abrupt transition in velocity occurs at the interface.

3. Experiments and observations

3.1. *Experiments*

The apparatus and experimental techniques have already been described in I. The tube used is made of Perspex and is 183 cm in length, 3 cm in depth and 10 cm in width. The experiments have the advantage of avoiding the inlet disturbances which may occur in continuous flow experiments; also the velocity distribution is easily predicted. They suffer from the disadvantage that it is difficult to mount measuring probes in the flow without causing significant disturbances, since the flow is not unidirectional past a probe fixed in the tube and disturbances to the flow carried 'downstream' by the fluid in the neighbourhood of the probe may be carried 'upstream' in the return flow as they spread. Moreover, very small probes appear to cause large disturbances (see I, p. 701).

The fluids used in these experiments were water and a lighter mixture of carbon tetrachloride and commercial paraffin (kerosene) commonly used for paraffin heaters. The tube was completely filled with the fluids, which were of equal depths, 1·5 cm, and after allowing the fluids to settle, one end was sharply raised and the resulting motion of the interface recorded on ciné film running at about 70 frames/sec. The film speed was found by filming a stop watch, and the times in the experiments assessed by counting the film frames. The tube was filmed directly from the side and indirectly from above by means of a mirror set above the tube. The angle of tilt of the tube was varied between 4 and 12°. For smaller angles the time before instability occurred was rather long, whilst for larger angles instability occurred so rapidly that it was difficult to measure the time of onset with any accuracy. The times of the onset of instability were taken to be the sum of half the time taken to tilt the tube (usually about $\frac{1}{4}$ sec) and the time measured from the instant the tube reaches its tilted position until that at which instability could first be detected (this is the time t_1, in I). The first signs that waves were growing was the appearance of transverse bands of light across the tube viewed from above through the mirror. Soon afterwards the waves were seen to grow with the same periodicity as the bands. The bands confirmed the two-dimensional nature of the waves. The formation of the bands before the waves could be seen directly was probably due to the refraction of light, which provided illumination from the side, by very small wave slopes. The

wavelengths were measured from the projected ciné film when the wave amplitudes were quite large. No change in wavelengths was observed between the time that the bands were first noticed and the time when the waves reached their maximum amplitudes.

The surface tension at the interface is the quantity most difficult to measure. The 'drop' method was used with corrections made using the data to be found in Davies & Rideal (1963, p. 45). No method of cleaning the interface in the experiments was used, but care was taken to keep the liquids as clean as possible. The measured values of interfacial tension, γ, are probably good to within 10 %, and fortunately γ appears in expressions having a small fractional exponent in the theory, and thus the errors are not serious.

3.2. *The onset of instability and the wave-number of the disturbance*

The times at which instability was first observed and those at which it is predicted to occur are compared in figure 6. The points marked indicate the observed times and the corresponding predicted times based on (2.27) with l given by (2.29) (r is sufficiently large for (2.29) to be a very good approximation). The horizontal lines indicate the scatter in the observed values. The predictions are good at small times, corresponding to large angles of tilt, but are lower than the observations at small angles of tilt. Two corrections have been applied to the predicted values and the result of these corrections is to raise the predicted values for the small angles of tilt to the points indicated by the arrows in figure 6. (The corrections are insignificant for large angles of tilt.) The first correction is for the effect of viscosity at the interface described in § 2.5, which raises the predicted value of the critical velocity difference, and therefore the time at which instability occurs. The second correction is for the value of the wave-number. The predicted values of l in the experiments for large r have a linear dependence on B and therefore on $(\tan\alpha)^{\frac{2}{3}}$ (see (2.29)), and the results for the measured wave-numbers are presented on a plot of $(l-1)$ $(=(k/k_c)-1)$ against $(\tan\alpha)^{\frac{2}{3}}$ in figure 7. One root-mean-square deviation in $(l-1)$ is indicated by the horizontal lines. The wave-numbers increase with $(\tan\alpha)^{\frac{2}{3}}$ as predicted, but are well below the predicted values falling for the most part near k_c. The probable errors in the measurements are not sufficient to account for this. It appears that the wave motion may 'lock in' to a wave-number near k_c at an early stage of the development of the waves and that the larger wave-numbers favoured by the acceleration are never able to grow as rapidly as predicted by the theory.† The value of l which is observed is thus below that value which minimizes t_{100} (see (2.27)), and thus slightly higher values of the predicted time of onset of instability corresponding to the observed values of l are appropriate. This is the second correction made to the predicted values of the time at which instability occurs.

The corrected predictions still fall below the observed times and an additional

† The wave-numbers observed are slightly greater than half those predicted, and it is possible that, rather than 'locking in' to a wave-number near k_c, an interaction process favouring waves of twice the predicted wavelength operates in the very early stages of growth, similar to that observed for miscible fluids at a late stage in the growth described in I (see p. 700).

factor may be that, because there is a decrease in the observed wave-numbers as the angle of tilt, α, is decreased (figure 7), the slope of the disturbances at comparable amplitudes decreases as α decreases. Since the waves are first observed by the refraction of light, caused by the slopes of the waves, it seems probable that waves growing at small α will be detected later relative to the predicted time than waves at a larger α. This view is supported by measurements made of the growth of the waves.

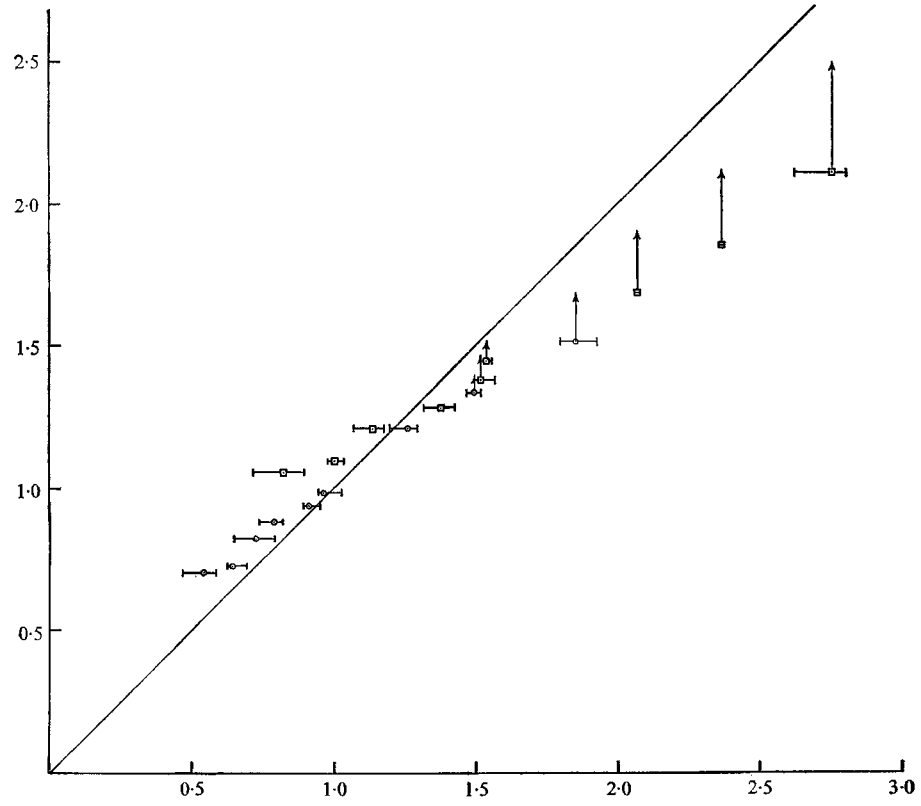

FIGURE 6. Comparison of observed and predicted times of onset of instability. The times predicted on the basis of (2.27) and (2.29) are marked with ⊙, corresponding to

$$(\rho_2-\rho_1)/(\rho_1+\rho_2) = 0{\cdot}124, \quad \gamma = 39{\cdot}9 \text{ dynes cm}^{-1},$$

or ⊡ corresponding to

$$(\rho_2-\rho_1)/(\rho_1+\rho_2) = 0{\cdot}074, \quad \gamma = 33{\cdot}4 \text{ dynes cm}^{-1}.$$

The arrows mark the corrected predictions as explained in the text. The horizontal lines indicate the scatter of observations about the points which each represent the mean of three experimental runs.

3.3. *The growth of waves*

The development of the waves and their shape is shown in figure 8 (plate 1). The growth of the waves has been examined by measuring the wave heights from the projected image of the waves from the ciné film. Accurate measurement was

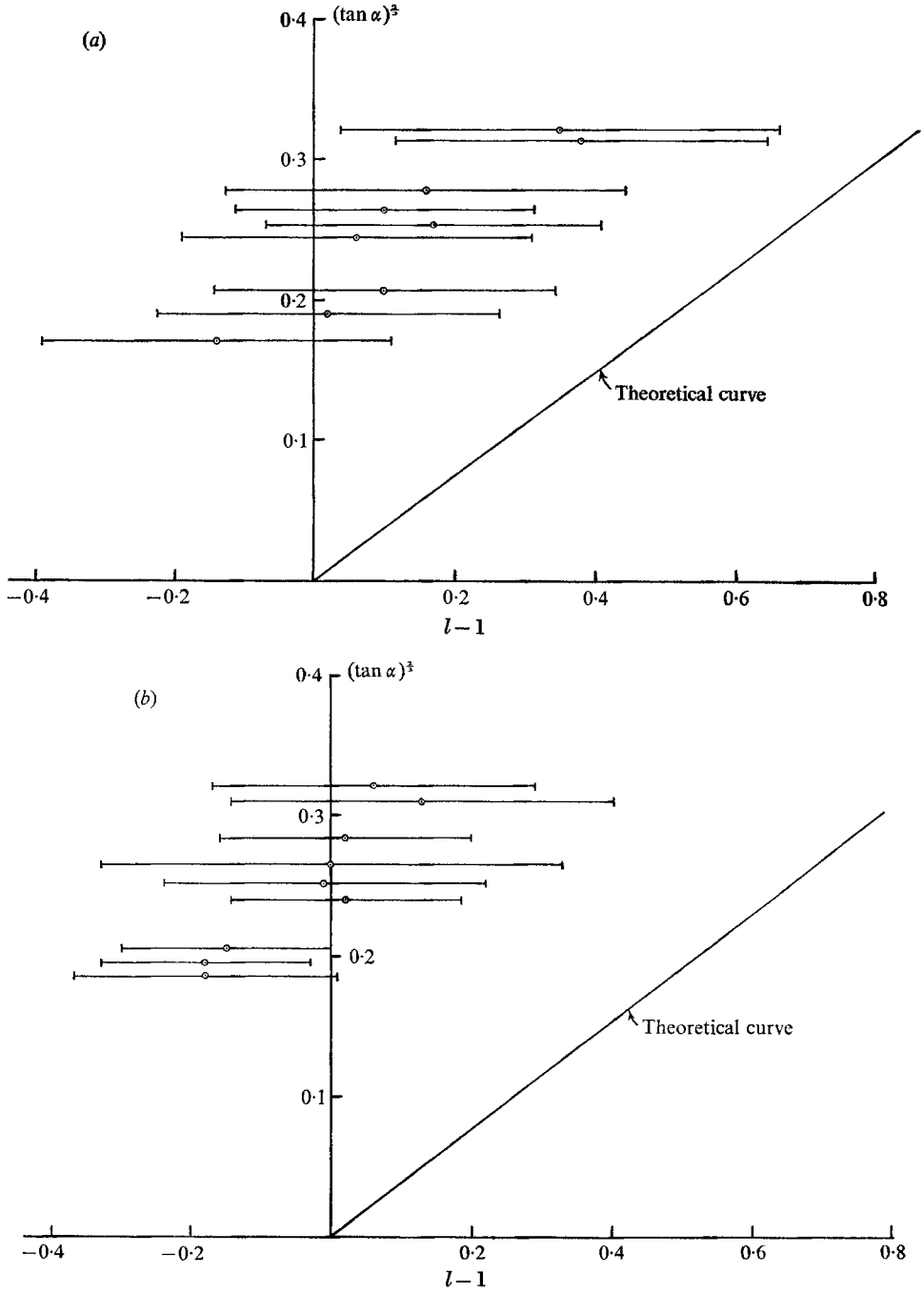

FIGURE 7. The variation of $l-1$ $(=(k-k_c)/k_c)$ with $(\tan\alpha)^{\frac{2}{3}}$ for

(a) $(\rho_2-\rho_1)/(\rho_1+\rho_2) = 0{\cdot}124$, $\gamma = 39{\cdot}9$ dynes cm^{-1}

and (b) $(\rho_2-\rho_1)/(\rho_1+\rho_2) = 0{\cdot}074$, $\gamma = 33{\cdot}4$ dynes cm^{-1}.

The points indicate the mean observed values and the horizontal lines indicate one root-mean-square deviation from the mean.

not possible during the early part of the wave growth when the wave slopes† were less than 0·1 and the wave amplitudes less than 1 mm, and only the growth of the wave crest has been examined since the wave trough was obscured during the early parts of the growth by the meniscus at the front of the tank. The observations of the position of the trough in the developed wave for

$$(\rho_2-\rho_1)/(\rho_1+\rho_2) = 0{\cdot}124$$

indicate that there was no difference which could be measured between the crest height above, and trough depth below, the initial position of the interface, and that the wave profile was almost symmetrical about the initial position of the interface. Between slopes of 0·1 and 0·2 the growth-rate gradually increased. A slope of 0·2 was reached at a time of about $1{\cdot}2t_1$, where t_1 is the time at which instability occurred, and thereafter an almost constant growth-rate was maintained up to wave slopes of 1·2 (reached at about $1{\cdot}45t_1$) when small-scale irregularities became evident in the wave profile and the rate of growth decreased. At these large slopes the effect of the boundaries of the tube was probably considerable, the wave filling about $\frac{1}{3}$ or more of the total depth of the tube. The value of the constant growth-rate increased as the angle of tilt, α, increased (and therefore as t_1 decreased) and table 1 shows some of the measured values during one set of experiments. It is noticed that the time at which the wave slope reaches a particular value is more nearly a constant multiple of the *predicted* value of t_1 rather than the observed value of t_1, and this suggests that perhaps the trend of points in figure 6 to values of greater than those predicted is partly the result of errors made in the determination of the time of onset of instability.

$\sin\alpha$	$\frac{d}{dt}(ak)$ ($\sec^{-1}$)
0·072	5·1
0·093	6·6
0·127	7·1
0·147	8·4
0·180	12·8

TABLE 1. The rate of change of wave slope, $d/dt(ak)$ during the period of constant growth-rate at different angles of tilt, α, for $(\rho_2-\rho_1)/(\rho_1+\rho_2) = 0{\cdot}124$ and $\gamma = 39{\cdot}9$ dynes cm^{-1}

By observing the points at which the wave profile intersected the initial position of the interface, a small mean wave motion down the slope was noticed. The observations were scattered and not sufficient to detect any variation of the wave speed with α or at different wave slopes. The mean speed was 2·6 cm $\sec^{-1}$ for $\delta = (\rho_2-\rho_1)/(\rho_1+\rho_2) = 0{\cdot}124$, $\sin\alpha$ between 0·072 and 0·180, and wave slopes between 0·2 and 1·2. From (2.15), (2.17) the predicted phase speed of the waves is

$$c = 2\beta t/k = \delta^2 g \sin\alpha t$$

† The wave slope is taken as ak, where a is the height of the crest above the initial position of the interface.

in a direction down the slope. For $\sin\alpha = 0{\cdot}127$, $\delta = 0{\cdot}124$, and $t = 1{\cdot}24$ sec (corresponding to the time at which a wave slope of 0·7 was reached in the experiments with those values of $\sin\alpha$ and δ) we find that $c = 2{\cdot}38\,\mathrm{cm\,sec^{-1}}$, in good agreement with the observed mean value.

At times later than $1{\cdot}45t_1$, the interface became very irregular, sometimes being broken and drops of one fluid being produced in the other,† but frequently it eventually settled to a pattern containing waves of length about three times those of the original disturbance with smaller irregular waves superimposed.

4. Final remarks

The experiments made in the tilted tube provide the possibility of testing some of the theoretical predictions which have been made about the onset of turbulence in a stratified shear flow, and serve to emphasize the importance of the study of time-dependent flows.

Quite good agreement is found between the times at which instability is first observed in the experiments, and those predicted by a theory based on Kelvin–Helmholtz instability. The observed wave-numbers show the predicted increase with the angle of tilt of the tube resulting from the effects of the accelerating flow, but are somewhat smaller than the predicted values. This is not entirely surprising in view of the reservations about the accuracy of the predictions made in § 2.3, and it is possible that the effects of finite amplitude, neglected in this paper, become important at an early stage of wave development. The possibility of Tollmien–Schlichting instability at the interface has not been discussed. The agreement found between the observed and predicted times suggests that Kelvin–Helmholtz instability plays a part in the wave development. Whether or not it is a dominant role is not clear.

Further experiments have been made on the instability of two miscible fluids with a diffuse interface, and the results compare favourably with theory; these will be published later.

I am grateful for the assistance of Mr Richard Soulsby and Mr Paul Hutt in the making of the experiments, and to Mr Arnold Madgwick for his advice and help in photography.

Appendix A. Disturbances in the accelerating flow

We shall suppose that $\xi = \eta(t)\,e^{ikx}$ and that

$$\phi_1 = \psi_1(t)\cosh k(z-h)\,e^{ikx}, \quad \phi_2 = \psi_2(t)\cosh k(z+h_2)\,e^{ikx},$$

to satisfy (2.8) and (2.10), where the real parts of terms appearing on the right-hand sides are to be taken. (For a random initial disturbance a sum of terms like those appearing on the right-hand sides may be taken, for various wave-numbers k, in the usual way.)

† These drops were typically about 5 mm in diameter or less.

At the interface, the linearized forms of (2.11) become

$$\frac{d\eta}{dt}+\frac{ik(\rho_2-\rho_1)\,g\sin\alpha\,h_2 t}{\rho_1 h_2+\rho_2 h_1}\eta=-k\psi_1\sinh kh_1 \tag{A 1}$$

and

$$\frac{d\eta}{dt}-\frac{ik(\rho_2-\rho_1)\,g\sin\alpha\,h_1 t}{\rho_1 h_2+\rho_2 h_1}\eta=k\psi_2\sinh kh_2, \tag{A 2}$$

whilst (2.14) becomes

$$p_i(z=\xi)=\rho_i\Big\{A_i(t)+\frac{(-1)^i(\rho_2-\rho_1)\,gh_j\sin\alpha}{\rho_1 h_2+\rho_2 h_1}(x+ik\psi_i\cosh kh_i\,e^{ikx})$$
$$-\frac{\partial\psi_i}{\partial t}\cosh kh_i\,e^{ikx}-gx\sin\alpha-g\eta\cos\alpha\,e^{ikx}\Big\}\quad(i\neq j) \tag{A 3}$$

evaluated at $z=0$. Now from (2.13), at the interface,

$$p_1-p_2=\gamma/R=\gamma\frac{\partial^2\xi}{\partial x^2} \tag{A 4}$$

to a first approximation. Hence substituting from (A 3) and equating coefficients of e^0, e^{ikx},

$$\rho_1 A_1=\rho_2 A_2 \tag{A 5}$$

and

$$\rho_1\frac{\partial\psi_1}{\partial t}\cosh kh_1-\rho_2\frac{\partial\psi_2}{\partial t}\cosh kh_2+i\frac{(\rho_2-\rho_1)\,kgt\sin\alpha}{\rho_1 h_2+\rho_2 h_1}$$
$$\times(\rho_1 h_2\psi_1\cosh kh_1+\rho_2 h_1\psi_2\cosh kh_2)=[\gamma k^2+(\rho_2-\rho_1)\,g\cos\alpha]\,\eta. \tag{A 6}$$

Substituting for ψ_1 and ψ_2 from (A 1) and (A 2) we find

$$\left(\frac{\rho_1}{T_1}+\frac{\rho_2}{T_2}\right)\frac{d^2\eta}{dt^2}+\frac{2ikt(\rho_2-\rho_1)\,g\sin\alpha}{\rho_1 h_2+\rho_2 h_1}\left(\frac{\rho_1 h_2}{T_1}-\frac{\rho_2 h_1}{T_2}\right)\frac{d\eta}{dt}$$
$$+\left\{(\rho_2-\rho_1)\,gk\cos\alpha+\gamma k^3+\frac{ik(\rho_2-\rho_1)\,g\sin\alpha}{\rho_1 h_2+\rho_2 h_1}\left(\frac{\rho_1 h_2}{T_1}-\frac{\rho_2 h_1}{T_2}\right)\right.$$
$$\left.-\frac{t^2k^2(\rho_2-\rho_1)^2g^2\sin^2\alpha}{(\rho_1 h_2+\rho_2 h_1)^2}\left(\frac{\rho_1 h_2^2}{T_1}+\frac{\rho_2 h_1^2}{T_2}\right)\right\}\eta=0,$$

where

$$T_i=\tanh kh_i\quad(i=1,2),$$

and if now

$$\eta=N(\tau)\,e^{i\beta t^2}, \tag{A 7}$$

where

$$\tau=\left[\frac{2kg\sin\alpha(\rho_2-\rho_1)\,(h_1+h_2)\sqrt{(\rho_1\rho_2T_1T_2)}}{(\rho_1 h_2+\rho_2 h_1)\,(\rho_1T_2+\rho_2T_1)}\right]^{\frac{1}{2}}t \tag{A 8}$$

and

$$\beta=-\frac{k(\rho_2-\rho_1)\,g\sin\alpha(\rho_1h_2T_2-\rho_2h_1T_1)}{2(\rho_1T_2+\rho_2T_1)(\rho_1h_2+\rho_2h_1)}, \tag{A 9}$$

the equation reduces to the form

$$\frac{d^2N}{d\tau^2}-\{a+\tfrac{1}{4}\tau^2\}N=0, \tag{A 10}$$

where $$a = -\frac{[\gamma k^2 + (\rho_2 - \rho_1) g \cos\alpha](\rho_1 h_2 + \rho_2 h_1)\sqrt{(T_1 T_2)}}{2g \sin\alpha(\rho_2 - \rho_1)(h_1 + h_2)\sqrt{(\rho_1 \rho_2)}}. \tag{A 11}$$

Appendix B

Given a three-dimensional disturbance to the basic flow, it may be shown that there is a two-dimensional disturbance in the same flow which will increase its amplitude by (say) 100 times more rapidly than will the three-dimensional disturbance. This is an extension of the well-known Squires theorem, and leads us to expect that the onset of instability will be characterized by two-dimensional disturbances, as is indeed observed. The proof of this result is outlined below in the case when $h_1 = h_2$.

For a three-dimensional disturbance the displacement of the interface $\xi(x, y, t)$ may be written

$$\xi(x, y, t) = \mathscr{R}\{N(\tau_1) \exp[i(k_1 x + k_2 y + \beta_1 t^2)]\},$$

where $$\tau_1 = 2\left[\frac{k_1(\rho_2 - \rho_1) g \sin\alpha \sqrt{(\rho_1 \rho_2)}}{(\rho_1 + \rho_2)^2}\right]^{\frac{1}{2}} t$$

and $$\beta_1 = \tfrac{1}{2} k_1 \left(\frac{\rho_2 - \rho_1}{\rho_1 + \rho_2}\right)^2 g \sin\alpha.$$

$N(\tau_1)$ satisfies the equation

$$\frac{d^2 N}{d\tau_1^2} - (a_1 + \tfrac{1}{4}\tau_1^2) N = 0,$$

where $$a = -\frac{k}{k_1} \frac{\gamma k^2 + (\rho_2 - \rho_1) g \cos\alpha}{4g \sin\alpha(\rho_2 - \rho_1)\sqrt{(\rho_1 \rho_2)}} \tanh kh,$$

and $$k^2 = k_1^2 + k_2^2.$$

(These equations replace equations (2.15)–(2.19).)

The time, $t_{100}^{(1)}$, at which 100-fold growth now occurs is given by

$$t_{100}^{(1)} = A \left\{ \left[\left(\frac{lr^2}{k_1^2 h_2}\right)(1 + l^2) \tanh lr \right]^{\frac{1}{2}} + \frac{B}{\left[l^2 \left(\frac{k_1 h}{r}\right)(1 + l^2) \tanh lr \right]^{\frac{1}{6}}} \right\},$$

where A, B, l, r are as given before; see (2.27). For a given flow $t_{100}^{(1)}$ decreases as k_1 increases, and has its smallest value when $k_1^2 = k^2$ and $k_2 = 0$. Hence the disturbance which is amplified most rapidly is two-dimensional.

Appendix C. Comparison with a quasi-steady approximation

We wish to compare the growth of disturbances as predicted by solutions of (2.18) with that predicted by (2.5) when ΔU has its instantaneous value at time t (the quasi-static approximation). When

$$\Delta U = \frac{2(\rho_2 - \rho_1) g \sin\alpha t}{\rho_1 + \rho_2}$$

(the difference $U_1 - U_2$ in (1.2)), the part of p in (2.5) not included in the curly brackets is,

$$\frac{ik(\rho_2-\rho_1)^2 gt\sin\alpha}{(\rho_1+\rho_2)^2},$$

which is equal to $2\beta t = (kc)$, when β is given by (2.17) with $h_1 = h_2$. Hence the quasi-steady approximation predicts correctly the phase speed of the disturbance.

The expression in the curly brackets in (2.5) becomes

$$4\left\{\frac{kg\sin\alpha(\rho_2-\rho_1)\sqrt{(\rho_1\rho_2)}}{(\rho_1+\rho_2)^2}\right\}\left(\frac{\tau^2}{4}+a\right)^{\frac{1}{2}},$$

where we have replaced g in (2.5) by $g\cos\alpha$ corresponding to the reduced effects of gravity, and thus the amplitude $|\eta|$ of the disturbance at the interface in the quasi-static approximation is given by

$$\frac{1}{|\eta|}\frac{d|\eta|}{d\tau} = \left(\frac{\tau^2}{4}+a\right)^{\frac{1}{2}}. \tag{C 1}$$

The solution of (C 1) is

$$|\eta| = |\eta_0|\frac{\exp\left\{\frac{\tau}{2}\left[a+\frac{\tau^2}{4}\right]^{\frac{1}{2}}\right\}}{\left\{\frac{\tau}{2\sqrt{(-a)}}+\sqrt{-\left(1+\frac{\tau^2}{4a}\right)}\right\}^{-a}},$$

where $|\eta| = |\eta_0|$ when $\tau = 2\sqrt{(-a)}$. With the approximation

$$4\sqrt{(-a)} \geqslant \tau - 2\sqrt{(-a)} \geqslant 0, \tag{C 2}$$

$$|\eta| = |\eta_0|\exp\left(\tfrac{2}{3}S_1^{\frac{3}{2}}\right),$$

where $s_1 = (-a)^{\frac{1}{2}}[\tau - 2\sqrt{(-a)}]$, and tenfold growth occurs at $s_1 = 2{\cdot}28$, 100-fold growth at $s_1 = 3{\cdot}73$. s_1 is equal to s and the growth is but slightly more rapid than predicted by solutions of (2.18) (see (2.21) and following) which had 100-fold growth at $s = 3{\cdot}83$.

For very large values of $\tau^2/(-4a)$, solutions of (2.18) are

$$V(a,\tau) \sim \sqrt{\left(\frac{2}{\pi}\right)}\frac{\exp(\tau^2/4)}{\tau^{(-a+\frac{1}{2})}},$$

whilst solutions of (C 1) are

$$|\eta| \sim \sqrt{\left(\frac{2}{\pi}\right)}\frac{\exp(\tau^2/4)}{\tau^{-a}}.$$

Thus the quasi-static approximation gives somewhat larger amplitudes than those predicted by the exact theory.

Detailed comparison of the solutions of (2.18) and (C 1) shows that the time of 100-fold growth is underestimated but is predicted by the quasi-static approximation to better than 10 % even without the approximation (C 2).

REFERENCES

ABRAMOWITZ, M. & STEGUN, A. 1965 *Handbook of Mathematical Functions*. New York: Dover.

BENJAMIN, T. B. 1960 *J. Fluid Mech.* **9**, 513.

BENJAMIN, T. B. 1963 *J. Fluid Mech.* **16**, 436.

DAVIES, J. T. & RIDEAL, E. K. 1963 *Interfacial Phenomena*, 2nd ed. New York: Academic.

HOLMBOE, J. 1962 *Geofys. Public.* **24**, 67.

KELVIN, LORD 1871 *Phil. Mag.* **42**, 368, and *Mathematical and Physical Papers* **4**, 76.

LANDAHL, M. T. 1962 *J. Fluid Mech.* **13**, 609.

LOCK, R. C. 1954 *Proc. Camb. Phil. Soc.* **50**, 105.

SCHLICHTING, H. 1955 *Boundary Layer Theory*. London: Pergamon.

THORPE, S. A. 1968 *J. Fluid Mech.* **32**, 693.

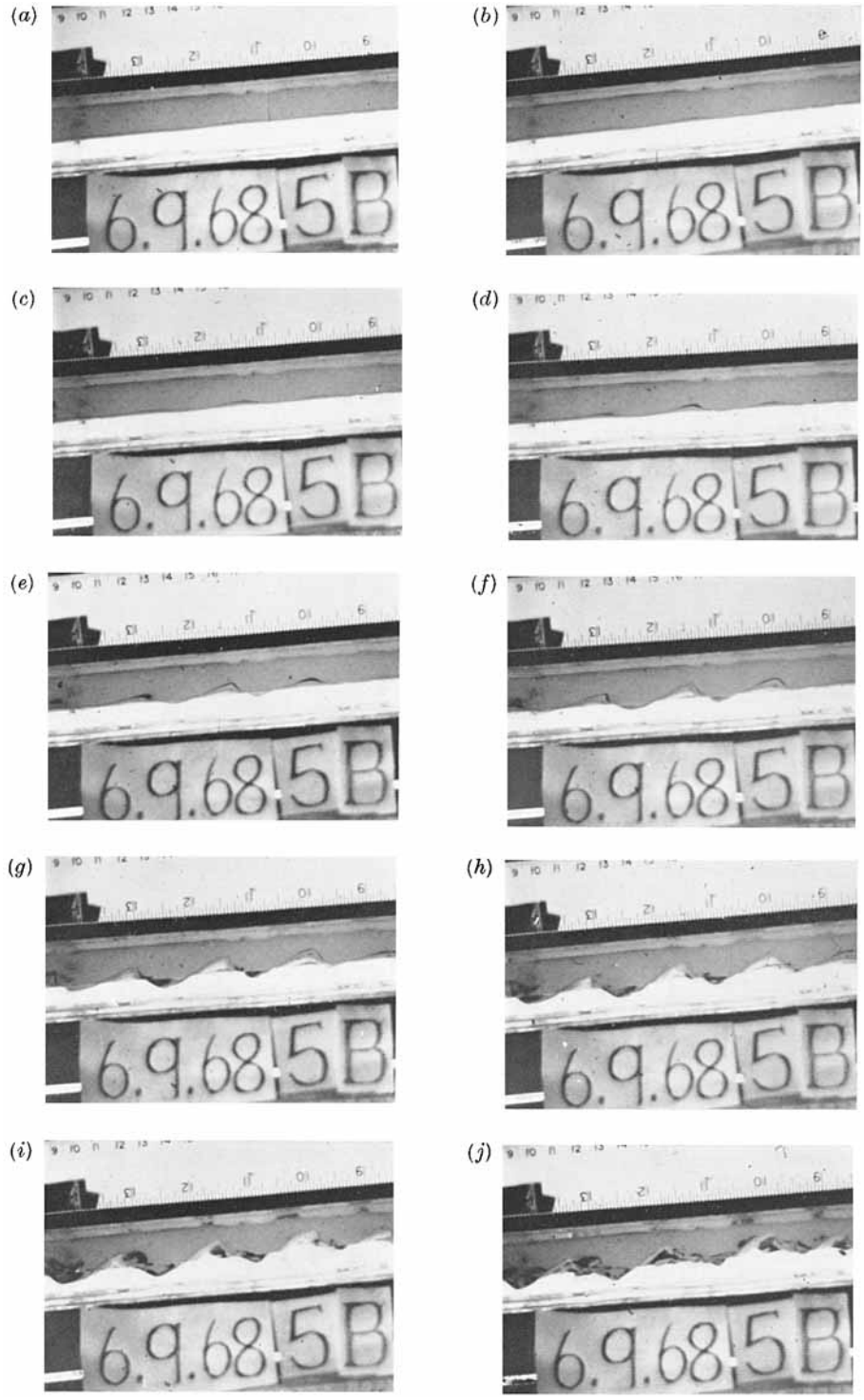

FIGURE 8. The growth of waves. The photographs are separated by 0·059 sec, the first (*a*) being 1·88 sec after the tube had been tilted.

$$(\rho_2-\rho_1)/(\rho_1+\rho_2) = 0{\cdot}124, \quad \gamma = 39{\cdot}9 \text{ dynes cm}^{-1}, \quad \sin\alpha = 0{\cdot}072.$$

The lower scale is in inches.

(*Facing p.* 48)